



IRRADIATED GOLD NANOPARTICLES FOR LOCALISED HYPERTHERMIA APPLICATIONS

V. Timchenko*

School of Mechanical and Manufacturing Engineering, UNSW Sydney, Sydney, Australia

ABSTRACT

Gold nanoparticles (GNP) aided hyperthermia has demonstrated promising results in the treatment of cancer. In this study, the impact of GNP clustering on the optical properties and heating capability of GNP aggregates in acidic solutions with pH levels close to cancer tissues has been investigated experimentally and numerically. It was found that localized heat generation could be significantly enhanced (up to 60.0 °C) when acidic solutions were illuminated by a near infrared light source. In addition, the heat transfer between GNPs and Tethered Bilayer Lipid Membranes (tBLMs) was numerically modelled to understand the effects of GNP hyperthermia on living cells membranes. The predicted temperature change was compared with the variation of membrane conductance of the tBLMs. The correlation of temperature change with an increase in membrane conductance suggests that heat transfer induces the creation of transient membrane pores and/or induces existing intrinsic membrane pores to be widened.

1. INTRODUCTION

The usage of heat as a method of treating diseases has been known in different cultures since ancient times. These days, thermal therapy is a potential treatment for destroying radio-resistant cancer cells as well as targeted treatment for infections. By using mild hyperthermia therapy, tissues are heated to a temperature within the range 39 °C to 45 °C [1]. At this temperature, properties of specific tumour tissues can be gradually altered because it has a lower heat tolerance than normal cells [2].

While thermotherapy has shown promising clinical results, it is difficult to control the heat generation and temperature distribution in diseased tissues and not to overheat surrounding healthy tissues. Gold nanoparticles (GNPs) have emerged as a new class of targeted hyperthermia treatments because of their biocompatibility and strong optical resonant absorption of near infrared (NIR) light in the so-called optical therapeutic window [2–4]. This therapeutic window stems from the fact that the human skin tissues only weakly absorb light with wavelengths between 650 nm to 900 nm. Therefore, NIR light can optically penetrate biological tissues and excite the GNPs embedded inside superficial tumours to generate localized heating. The advantage of this approach is that particles can be conjugated to specific antibodies or targeting ligands which, in turn, penetrate leaky tumour blood vessels to selectively target cancerous cells [5].

As the peak of this resonance absorption can be tuned depending on the size and shape of GNPs [6], different types of GNPs including nanospheres, nanoshells and nanorods have been explored [6-8]. Using cells targeted with spherical GNPs, Pissuwan et al. [9] showed that aggregation of the GNPs has a beneficial effect in killing protozoan parasite cells because it red-shifts their peak optical extinction towards wavelengths at which human tissue is more transparent and increases the absorption of light. The benefit of such an aggregation-induced red-shift of a surface plasmonic resonance (SPR) for selective heating was also observed by Hainfeld et al. [10] where it was shown that 15 nm diameter GNPs coated with lipolic acid aggregated at low pH, such as within tumours, whilst in surrounding normal tissue and blood they were not aggregated and therefore did not produce significant heating because of poor light absorption. The impact of GNP clustering on the optical properties of GNP aggregates is investigated in the present study, both experimentally and numerically, to provide an insightful understanding on the heating efficiency of complex GNP configurations in solutions with different pH levels.

*Corresponding Author: v.timchenko@unsw.edu.au

In our earlier works [11-12] we developed the models of the radiative heat transfer in a medium containing highly scattering and weakly absorbing tissues and highly absorbing and weakly scattering GNPs and studied the heat transfer between the GNPs and superficial tissues. To make a further step towards clinical applications and to understand the effects of GNP hyperthermia on living cells membranes, in the present paper, the heat transfer between GNPs and the Tethered Bilayer Lipid Membranes (tBLMs) are numerically modelled. The predicted results have been compared against experimental data obtained as a part of a collaborative research project which studied the disruption of lipid bilayers due to the heat generation of laser-irradiated gold nanospheres (GNSs) adjacent to the tBLMs. The technology developed by Prof. Valenzuela (the University of Technology Sydney) and Prof. Cornell (SDx Tethered Membranes Pty. Ltd.) [13-14] was applied in the experiment.

2. OPTICAL PROPERTIES OF NANOPARTICLES

To calculate a heat generation due to absorbed radiation power when nanoparticle solutions are exposed to NIR light, the radiation transfer problem has to be solved first. According to Dobmbrovsky [15], the absorption and scattering coefficient of the solution containing spherical nanoparticles with radius r can be calculated using Equation (1):

$$\alpha = \alpha_o + 0.75f_v \frac{Q_{abs}}{r} \quad \sigma_s = \sigma_{s,o} + 0.75f_v \quad (1)$$

where α and α_o is the absorption coefficient of the solutions and base fluid. σ_s and $\sigma_{s,o}$ is the scattering coefficient of the solutions and base fluid. f_v is the volume fraction of the GNPs in the solution, Q_{abs} and Q_{sca} are the absorption and scattering efficiency.

The amount of absorption and scattering is usually identified by the absorption and scattering coefficients C_{abs} and C_{sca} of the GNP configuration. The total amount of absorption and scattering is the extinction, which is expressed in the term of the extinction cross section $C_{ext} = C_{abs} + C_{sca}$. The dimensionless efficiency factors of these optical properties are commonly used as specified below:

$$Q_{ext} = \frac{C_{ext}}{\pi r^2} = Q_{abs} + Q_{sca} \quad (2)$$

The analytical expressions of the Mie theory for these efficiency factors and also for other characteristics of absorption and anisotropic scattering can be found in several texts, e.g. [15].

To calculate the optical properties of particles with arbitrary geometries the discrete dipole approximation (DDA) approach was introduced by DeVoe [16]. In this approach, the target is replaced by an array of point dipoles, known as polarizable points. The electromagnetic scattering problem for an incident periodic wave interacting with this array of point dipoles is then precisely solved. In the present study, a DDA code named Discrete Dipole Scattering (DDSCAT) 7.3 [17] has been applied to calculate the absorption and scattering efficiency of GNPs. Draine and Flatau [17] developed and validated the DDSCAT code based on Mie theory. This code has been adopted and validated in previous studies of GNPs and assemblies [18].

It is important to note that the scattering problem is characterized by the so-called diffraction or size parameter:

$$x = \frac{2\pi r}{\lambda} \quad (3)$$

where λ is the wavelength of the incident light.

In DDSCAT, the arbitrary target consists of N dipoles with lattice spacing d . V is the volume of the arbitrary geometry.

$$V = Nd^3 \quad (4)$$

The size of the target is characterized by the “effective radius” to calculate the arbitrary geometry.

$$r_{eff} = \left(\frac{3V}{4\pi}\right)^{1/3} \quad (5)$$

Since the solutions used in this study are aqueous, the refractive index of water, $1.33 + 0i$, is applied as the refractive index of the ambient at all wavelengths. More details for application of DDSCTAT to calculate the absorption and scattering efficiency of GNP configurations can be found in [8].

3. MODELLING OF HEAT GENERATION DUE TO ABSORBED RADIATION

The so-called radiative transfer equation (RTE) is considered in the traditional continuum theory. In the case of a negligible emission of the radiation by a scattering and absorbing medium, the RTE for randomly polarized radiation can be written as follows [19-20]:

$$\vec{\Omega} \nabla I_\lambda(\vec{r}, \vec{\Omega}) + \beta_\lambda I_\lambda(\vec{r}, \vec{\Omega}) = \frac{\sigma_\lambda}{4\pi} \int_{(4\pi)} I_\lambda(\vec{r}, \vec{\Omega}') \Phi_\lambda(\vec{\Omega}', \vec{\Omega}) d\vec{\Omega}' \quad (6)$$

The absorption coefficient, α_λ , the scattering coefficient, σ_λ , extinction coefficient and scattering, β , phase function, Φ_λ , depend on the coordinate \vec{r} . $\vec{\Omega}$ is unit vector of direction.

In our previous works [11, 12] we have simplified the RTE above and used the first-order approximation of the spherical harmonics method (P1) to solve the problem of laser irradiation of superficial tumors. To simulate experimental set-ups investigated in this work, the radiation transfer modelling was simplified further since the filtered incident light has a narrow band of wavelengths and the scattering is negligible in water-based solutions. Due to the negligible scattering coefficient of the GNP solutions, only the absorption coefficient computed from Equation (1) was adopted to calculate the absorbed radiation based on Beer-Lambert Law as written in Equation (7):

$$\frac{\partial I}{\partial z} = -\alpha I \quad (7)$$

where I is the light intensity and z is the coordinate along the direction of the incident light.

The radiation source term calculated from Equation (7) is:

$$-\nabla \cdot q_r = \alpha I \quad (8)$$

The energy transport in a biological system is usually expressed by the so-called bioheat equation. The bioheat equation developed by Pennes [21] is one of the earliest models for energy transport in tissues. Pennes assumed that the arterial blood temperature, T_b , is uniform throughout the tissue while the vein blood temperature is equal to the local tissue temperature T_t . The resulting transient energy equation is as follows:

$$\rho c \frac{\partial T_t}{\partial t} = \nabla(k \nabla T_t) + \rho_b c_b v_b (T_b - T_t) + W_m \quad (9)$$

where the second term on the right-hand side is responsible for the heat transfer due to arterial blood perfusion of rate v_b , and the last term W_m is the metabolic heat generation within the tissue. A more detailed model for heat transfer in human tissues should be based on two coupled energy equations for the tissue and artery blood with the spatial and time variation of arterial blood temperature is taken into account in such a model considered [22, 12].

In this work the transient energy-transport equation presented in Equation (10) was adopted to describe the diffusion of heat throughout the medium and predict the heat generation in irradiated GNP solutions.

$$\rho C_p \frac{\partial T}{\partial t} = \nabla k \nabla T - \nabla \cdot q_r \quad (10)$$

where ρ is the density, C_p is the heat capacity at constant pressure and T is the temperature of the solution with volumetric heat source due to absorbed radiation, $-\nabla \cdot q_r$, calculated from Equation (8).

4. EFFECT OF AGGLOMERATION OF NANOPARTICLES ON THEIR OPTICAL PROPERTIES AND HEATING EFFICIENCY

4.1 Optical properties of GNP solutions with various pH values

As mentioned above that aggregation of the gold NPs has a beneficial effect because it red-shifts their peak optical extinction towards wavelengths at which human tissue is more transparent and increases the absorption of light. To study this effect Peng et al. [23] produced GNP aggregations by controlling the pH value of the solutions. GNP aggregates were found when the base fluid of the solution had a pH value of 6.5. Based on Peng et al.'s experiment [23], in our work ([24]) we predicted the distribution profile of GNPs in a $1.5 \mu\text{m} \times 1.5 \mu\text{m}$ observation window in the acidic solution and validated their prediction by comparing the calculated optical properties of GNPs in the region with the measured optical properties obtained in [23].

Based on the results of Li et al. [24] on the structures of particle aggregates present in acidic solutions (Table 1) the weight averaged absorbance was calculated and compared with the experimental results obtained by Peng et al. [23] for water-based basic (pH = 9.4) and acidic solutions (pH = 6.5). The comparison of the results for both basic solutions with single spherical particle (monomers) and also for the aggregates in acidic solutions with particle volume fraction 0.05 showed very close agreement, which confirmed the predictions of the structures as shown in Figure 1. The dash line in Figure 1 is the weighted average of the absorbance of the structures shown in Table 1 (Monomer (29.7 %), Dimer (43.9 %), Trimer 3-0 (3.7 %), Trimer 3-1 (13.6 %), Tetramer 4-0 (0.5 %), Tetramer 4-1 (3.6 %) and Tetramer 4-2 (5.0 %)) cases, as predicted by the discrete phase simulations with slightly acidic base fluid [24]. The predicted plasmonic resonance can be seen to be in good agreement with the experimental results.

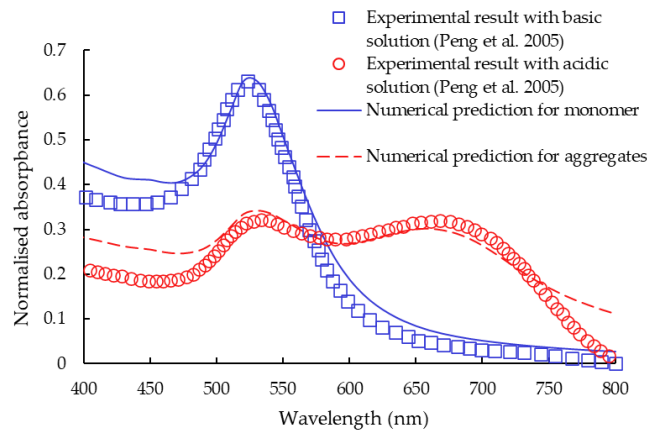



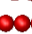



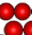


Figure 1. Normalized absorbance of solutions with GNP monomers (20nm diameter) and aggregations compared with experimental data [23] measured from nanoparticle solutions.

The absorption and scattering efficiencies of various GNP aggregation structures shown in Table 1 were calculated using DDA. As can be seen from the table, the configurations of Tetramer 4–2 showed the highest absorption efficiency at the wavelength of 640 nm.

Table 1. Absorption and scattering efficiencies of GNP configurations characterized by Li et al. [24] at 640 nm wavelength.

Particle Cluster Identifier	Particle Structure	Q_{abs}	Q_{sca}
Monomer		0.18	2.14×10^{-3}
Dimer		0.91	1.22×10^{-2}
Trimer 3-0		1.05	1.63×10^{-2}
Trimer 3-1		1.45	2.64×10^{-2}
Tetramer 4-1		1.57	3.67×10^{-2}
Tetramer 4-2		1.60	3.15×10^{-2}
Tetramer 4-3		1.29	2.20×10^{-2}
Tetramer 4-4		1.48	2.64×10^{-2}

The propagation direction of the incident light was assumed to be normal to the observation window. Two orthogonal polarisations of incident light were applied in the calculation. One with an electric field normal to the observation window, the other was parallel to it. In addition to the transverse surface plasmonic resonance (TSPR) observed at 520nm wavelength, a longitudinal surface plasmonic resonance (LSPR) within the so-called optical window of biological tissues (700 nm to 900 nm) was observed in both the experiment [23] and the numerical prediction for the GNP solution under acidic condition. This observation also agrees with the finding reported by Randrianalisoa et al. [25], where strong coupling regime with plasmon waves interaction was identified when the nanoparticles were sufficiently close or weakly overlapped.

To study the effect of pH on the heating efficiency the nanoparticle solutions with gold nanospheres (GNS) were gained from Sigma-Aldrich®. The dimension of the GNSs were 20 nm in diameter, which is in the range of suitability for accumulation in tumour without toxicity. The concentration of the purchased solution was 6.54×10^{11} particles/ml and the surface plasmon resonance (SPR) of the solution was suggested to be around 520 nm by the manufacturer. To control the pH of these nanoparticle solutions, 1M citric acid and 0.1M NaOH solutions were prepared and gradually added to the solutions using pipettes. The resulting pH value of the nanoparticle solution was measured by a pH meter. Transmission and reflection of GNS solutions with various pH values were measured by a spectrophotometer with an integrating sphere. The absorbance spectrum of each sample was calculated using Equation (11) and is shown in Figure 2. The transmittance of the 640 nm bandpass filter is also presented with a second y-axis.

$$Abs = \log_{10} \frac{P}{P_0} = 2 - \log_{10}(T' \times 100) = \epsilon lc = \frac{\alpha \times l}{2.303} \quad (11)$$

$$A'\% = 100\% - T'\% - R'\%$$

Where Abs is the absorbance of the sample, P is the light intensity the sample received and P_0 is the light intensity transmitted through the samples. The absorbance of the sample was logarithmic to the percentage of the transmitted light. ϵ , l and c are the absorptivity, path length and concentration of the sample. In this study, the dimension of the measured sample was $1 \times 1 \times 3.5 \text{ cm}^3$ (3.5 mL), so the path length was 1 cm. α is the absorption coefficient of the sample. The absorption coefficient of solutions obtained from the experiments was compared with results calculated by Equation (1). A , T and R are the absorption, measured transmission and reflection of the samples.

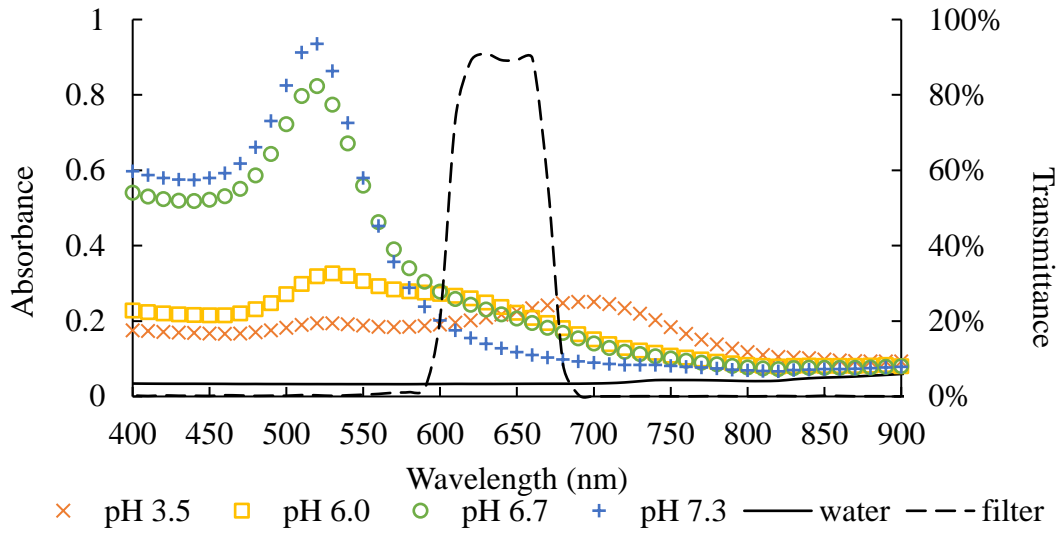


Figure 2 Absorbance of GNS solutions with various pH values.

4.2 Heat Generation in Irradiated GNS Solutions with different pH levels

A Hydrosun[®] 750 lamp with a water filter was used to irradiate the samples near their LSPR. Additional bandpass filters are selected based on the spectra measured using a Perkin Elmer[®] Lambda 1050 UV/Vis Spectrophotometer to further limit the radiation from the lamp to that of the optical window of biological tissues as shown in Figure 2. The specific light intensity of the Hydrosun[®] 750 lamp was previously analyzed in [26]. It should be noted that the Hydrosun[®] 750 lamp has been adopted in this experiment because it is used in clinical treatments as means to deliver a mild hyperthermia to the cancerous tissues, such as recurrent breast cancer [27].

The intensity of the radiation is calculated using the following equations:

$$I = \int_{\lambda_1}^{\lambda_2} q_{\lambda}^{\text{ext}}(\lambda) \times T(\lambda) d\lambda \quad (12)$$

where q_{λ}^{ext} is the spectral irradiance of the Hydrosun[®] 750 lamp at wavelength λ , $T(\lambda)$ is the transmittance of the filters (refer to Figure 2). The range limits λ_1 and λ_2 are also determined by the transmittance spectrum, while I represents the overall intensity transmitted through the filter from λ_1 to λ_2 wavelength. The intensity of the lamp is measured in present study using the Thorlabs[®] S305C thermal power sensor. The intensity of the lamp measured at the wavelength of NIR light is around 1.58 kW/m², which is in good agreement with the intensity values presented in [26].

The concentrated intensity of the lamp passing through a lens, measured at the same wavelength, was around 19.0 kW/m². The concentrated light source was applied in the thermal experiments to increase the intensity of the NIR light to ensure a more distinct, hence can be more accurately measured, temperature difference.

Figure 3 shows the schematic of the thermal experiment setup. During the experiment, the sample was placed in a water bath to limit heat loss. The temperature in the water bath was maintained at 37 °C to mimic human body temperature. The top of the sample was covered by clear wrap to reduce convection heat loss. As mentioned above, an optical bandpass filter was placed above the sample. Thermocouples were used to continuously measure the local temperature inside the sample and the water bath. The experimental data were captured by PicoLog[®] data logger.

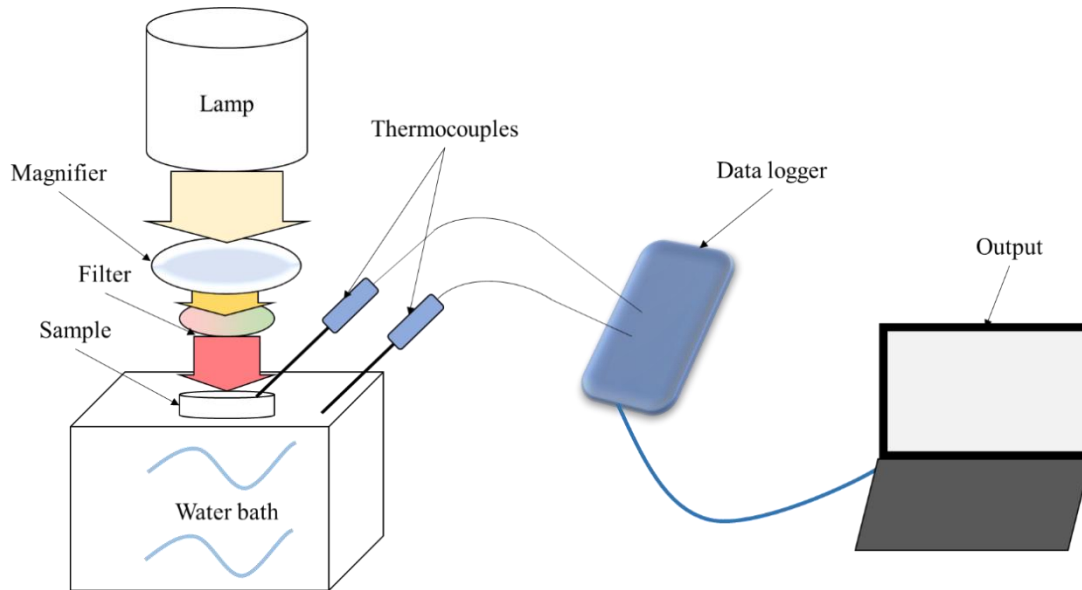


Figure 3. Schematic view of the thermal experiment.

The samples were exposed to the Hydrosun® 750 lamp with the 640-50 Filter for 600 seconds. The temperature change in the solutions were monitored till 200 seconds after the lamp was turned off.

To simulate the experiment described above an axisymmetric geometry with a diameter of 2.54 cm and a depth of 1 cm was modelled to predict the temperature change in the GNS solutions during the radiation. The absorption coefficients of samples at 640 nm wavelength were calculated by Equation (11) resulting in values of 55.27 m^{-1} and 29.94 m^{-1} for pH=6 and pH=7.3 correspondingly. The intensity of the filtered light source related to the transmission of the 640-50 filter shown in Figure 2 and the radiation flux of Hydrosun® 750 lamp was calculated by Equation (12). The power input in this case was around 8.66 Watts.

Since the top of the plate was covered by a layer of clear wrap, the boundary at the top surface was assumed to be insulated. The heat generation in the computational domain was caused due to a beam radiation, therefore the heat transfer model was time-dependent with a 600 seconds exposure to the radiative beam. Since the incident light was concentrated by a magnifier the profile of the radiative beam was modelled using Gaussian distribution.

The predicted temperature change during and after the radiation has been compared with the experimental result as presented in Figure 4. As can be seen, the predicted maximum temperature increase in both samples was similar to the measured value. The maximum temperature in the sample with a pH level of 6.0 was around $60 \text{ }^\circ\text{C}$ and reached a steady statue after 500 seconds exposure to the incident light. As under normal physiological conditions the pH of blood and tissue are controlled around pH 7.4, the difference in the maximum temperature of 7°C between solution with pH=7.3 and with pH=6.0 (close to cancerous tissues) can be beneficial for the GNP targeted hyperthermia treatment. The slight discrepancy of calculated and measured temperature occurred at the heating stage could be caused by the slightly overestimated absorption of light using Beer-Lambert law.

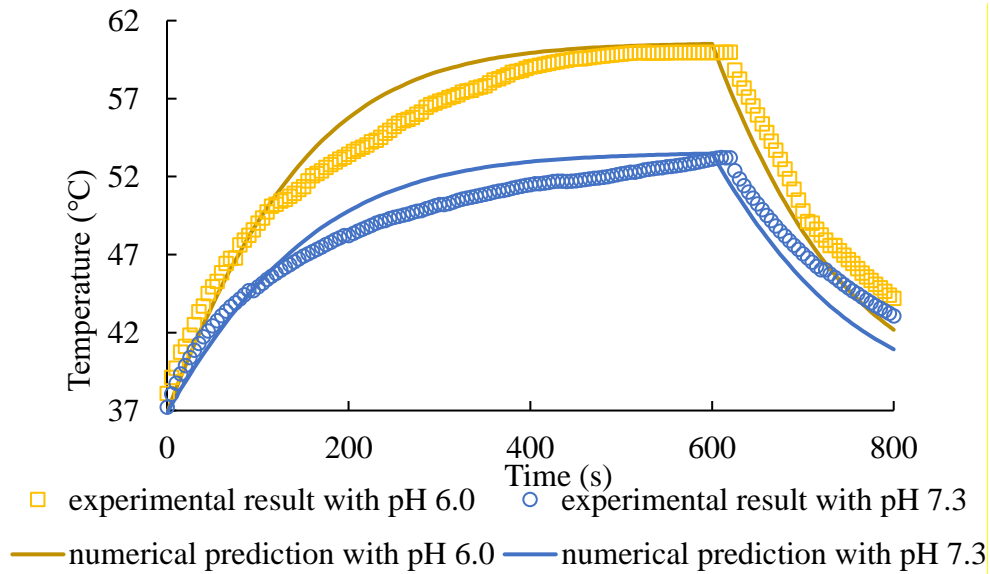


Figure 4 Calculated and measured temperature change in GNS solutions with different pH

5. HEAT TRANSFER BETWEEN GOLD NANOSPHERES AND TBLMS

5.1 Description of the tBLMs System

A tBLMs system was adopted in the experiment designed to imitate the natural environment of living cells membranes [13]. Figure 5(a) presents the structure of a typical tBLMs containing ion channels used to represent the functional membrane transport. As presented in Figure 5, some of the lipids are tethered to a gold electrode while others remained mobile in order to measure the conductance by an alternating current (A.C.) impedance reader. It was hypothesised that heat generated by the irradiated GNSs adjacent to the tBLMs will result in a change of conductance in the tethered membrane and thus can be measured through the ion-channel [13, 28-29].

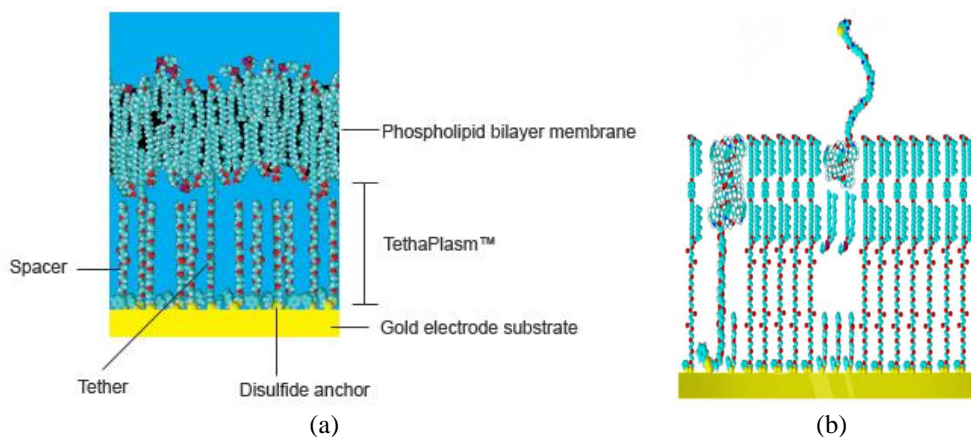


Figure 5 (a) Components of a tethered membrane attached to a gold surface, (b) the membrane contains an ion channel [29].

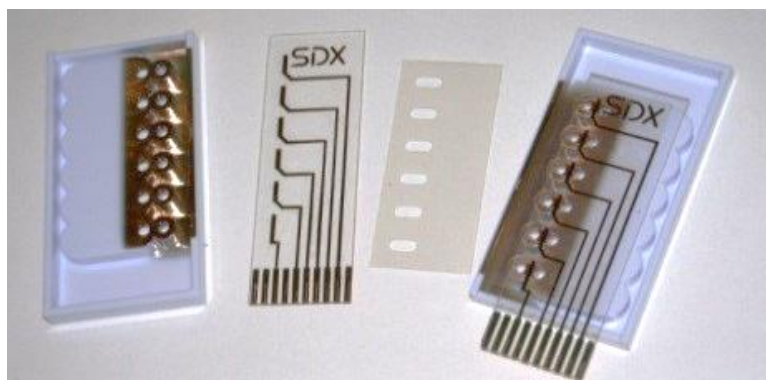


Figure 6 The tethaPlate™ to which the tethered membrane was attached [29].

The electrode to which the tBLMs were attached and a white (or clear) cartridge coated with a gold return electrical path are shown in Figure 6. To contain samples of GNPs, six test elements were formed when the cartridge and slide were assembled. The incident beam was directed either through the clear electrode or a clear version of the cartridge. Membrane conductance was monitored and recorded throughout and following the irradiation.

Streptavidin-conjugated GNPs with different concentrations were introduced to the liquid phase adjacent to the lipid bilayer membrane and irradiated by a 530 nm laser beam at the SPR of the GNSs. Electrical impedance spectroscopy was applied in the experiment to measure the variation in basal membrane ionic conduction caused by the heat generation of GNSs. Thus, the localised heating effect of GNS solution on tBLMs can be evaluated. The change in irradiated tethered membrane conduction was measured with and without GNSs. The experimentally recorded variations of the conductance in the samples with and without GNSs showed no difference when the laser light shone vertically above. However, when direction of laser beam was changed to the horizontal as shown in Figure 7 there were observed changes in the conductance between the cases with and without nanoparticles. A computational model was developed in this study to explain the experimental findings and to numerically investigate heat transfer phenomena in the system.

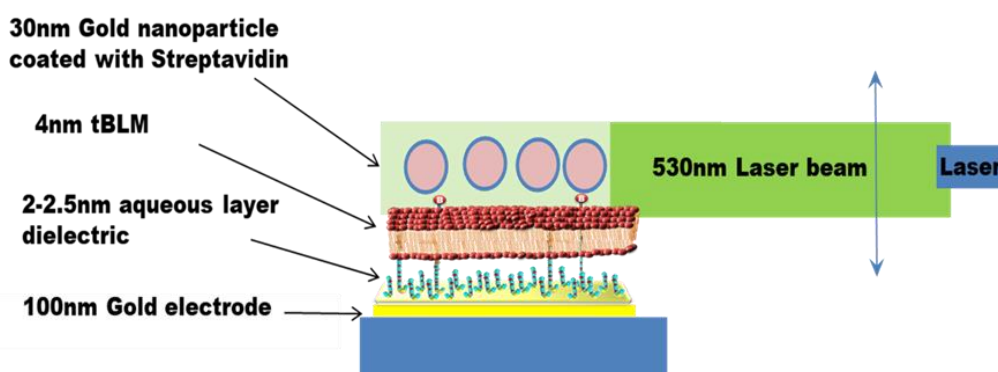


Figure 7. Schematic view of heated GNPs interface system [29].

5.2 Modelling the Heat Transfer in the tBLM System

A computational model was established based on the experiment described above. The GNSs were adjacent to the ion-channels and the distance between the channels was around 30 nm. Since the gap between GNSs was comparable to the size of GNSs, it was assumed that there was no clustering effect on the optical properties of GNSs.

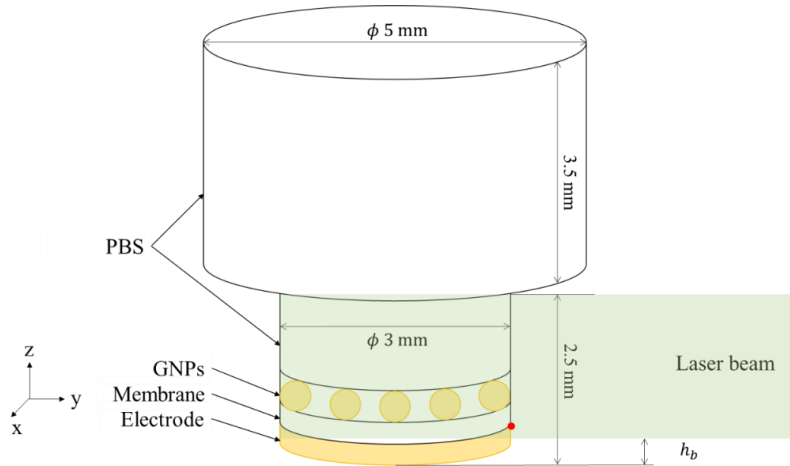


Figure 8 A sketch of the computational domain.

Figure 8 presents the locations of the components and the dimensions of the well geometry. h_b indicates the position of the incident beam. It should be noted that the incident light can be directed either vertically or horizontally, although Figure 8 only presents the situation when the laser beam shone horizontally on the side of the sample. The diameter of the incident light spot was 3 mm, same as the diameter of the bottom part of the well geometry. Therefore, it can be assumed that all GNSs attached to the membrane were irradiated by the laser.

The cartridge was made of plastic thus the walls around the test well were assumed to be thermally insulated. Since the top of the well was open to the air, a convective heat loss was applied to simulate the boundary condition at this surface. The heat transfer coefficient was assumed to be $10 \text{ W/m}^2 \cdot \text{K}$. The boundary condition of the bottom surface was also simulated by a convective heat loss, because the gold electrode had a high thermal conductivity, and it contacted the gold return electrical path which led outside the system as shown in Figure 6. Due to lack of the temperature measurements the heat transfer coefficient of the convective heat loss at the bottom surface was tuned to correlate the temperature change at the location indicated by the red dot in Figure 8 with measured conductance of the membrane and was assumed to be equal to $100 \text{ W/m}^2 \cdot \text{K}$.

The heat source due to absorbed radiation was incorporated into the energy equations, as described in Section 3. The heat transfer model was time-dependent with a 105 second exposure to the laser beam. The cooling stage after the laser was turned off was also predicted for 105 seconds. The radiative beam was modelled as a top-hat beam with the radius of the laser light spot being equal to 1.5 mm. The power of the laser was 135 mW.

Since the top surface of the gold electrode is rough, as presented in Figure 9(a), the optical properties of the electrode layer should be carefully treated. In the present computational model, the gold electrode was modelled into two layers. The top of the electrode was modelled as a 30 nm thick layer of 10×30 nm gold nanorods to mimic the rough surface. The bottom part of the electrode was modelled as a 70 nm gold film. The modelling of the electrode is demonstrated in Figure 9(b).

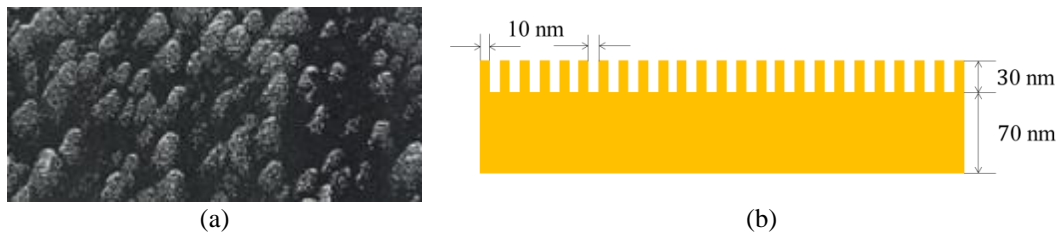


Figure 9 (a) An SEM image of the top surface of the gold electrode and (b) the characterised gold electrode with a rough surface.

Table 2 Dimension and optical properties of materials in the experimental sample.

Layer	Thickness in the Well (nm)	Absorption Coefficient (m^{-1})	
PBS	5.99×10^6	0.04 [31]	
GNS	30	4.7×10^7 [32]	
Membrane	6.5	242.5 [33]	
		Vertical Beam	Horizontal Beam
GNR	30	2.7×10^7	2.0×10^7
Film	70	6.2×10^7 [34]	1.7×10^5

Table 2 shows the thickness of each layer in the sample domain and the absorption coefficient of all components. Since the PBS solution was water based, the absorption coefficient of water was applied for the PBS solution [31]. The absorption coefficient of 30 nm GNS was taken from the results calculated by Jain et al. [32]. The optical properties of the blood cell membrane [33] were applied to model the biological membrane in the current study. The absorption efficiency of 10×30 nm GNR calculated by DDA was used to model the absorption of the top electrode layer. Axelevitch et al. [34] examined the optical properties of a gold film with a thickness of 74 nm. The results calculated by Axelevitch et al. [34] were adopted to model the 70 nm gold film for the vertical beam direction due to the similar dimension to those ones used in [34]. The absorption efficiency of the gold film was predicted using DDA for the horizontal beam direction.

5.3 Predicted Temperature Change in the tBLMs System

Since the gold electrode had a high absorption coefficient as shown in Table 2, cases with various incident positions or directions of the laser beam were computed to investigate the effect of the electrode on heat generation in the irradiated sample. The temperature change shown in the following figures was calculated at the point indicated by the red spot in Figure 8. As mentioned above, the variations of the conductance in the samples with and without GNSs showed limited difference in the experiment when the laser light was directed vertically. To explain this experimental finding, the temperature profiles presented in Figure 10a were predicted when the incident light was imposed vertically above the sample. The calculated maximum temperature increase from initial temperature 25 °C in the tethered membrane with GNSs was only slightly higher than without GNSs. The difference between the two predicted temperature profile was insignificant compared to the overall temperature increase, nearly 20 °C. It can be presumed that the variations of the conductance in the samples with and without GNSs were similar due to the insignificant difference of the temperature changes. The temperature change in Figure 10b also shows that the intensity absorbed by the gold electrode was notable because the temperature increased by nearly 20 °C in the membranes without the presence of GNSs.

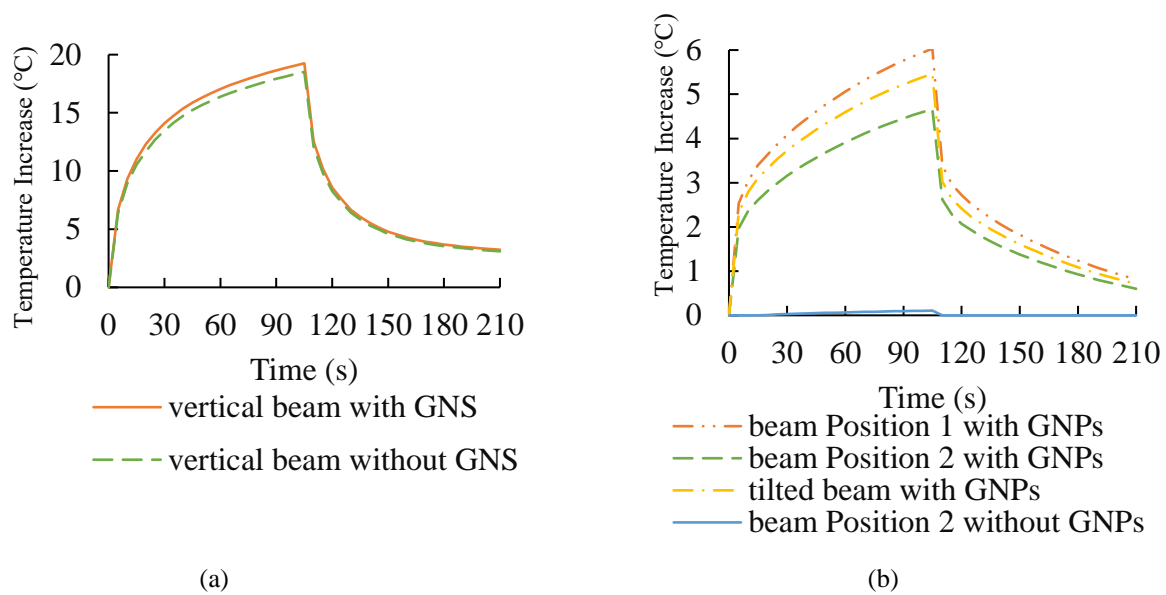


Figure 10 Temperature change in the tBLMs when the laser beam shone (a) vertically and (b) horizontally or slightly tilted

The results of the temperature change over time presented in Figure 10b were obtained when the incident light was directed horizontally at the side of the sample as shown in Figure 8. Two positions of the laser beam were modelled to analyse the impact of the electrode on the heat generation in the tBLMs system. Position 1 was at $h_b = 0 \text{ nm}$, where the electrode was exposed to the beam. Position 2 was at $h_b = 100 \text{ nm}$, where the electrode was not exposed to the light. The temperature change in the tBLMs was also calculated when the incident beam was tilted by 5 degrees at Position 2.

As shown in Figure 10 b, the temperature increased around 6 °C when the electrode was exposed to the incident light imposed horizontally. The temperature increased slightly lower when the laser was tilted by 5 degrees. The temperature increased by more than 4 °C when the electrode was not exposed to the laser. The lowest temperature increase occurred when the tBLMs were irradiated without GNSs and the laser beam was at Position 2. The cause of this insignificant temperature increase could be the intensity absorbed by the PBS solution and membranes.

The temperature increase in the membrane was much higher when the incident beam was directed vertically because the characterised gold electrode film had a higher absorption coefficient compared to the GNSs. The gold electrode layer was also thicker than the layer of GNSs. The absorption of the electrode was excluded when the beam was modelled at Position 2, so the heat generated in this case was only from the irradiated GNSs. As presented in Figure 10, when the electrode was not irradiated by the laser light, the temperature increased more than 4 °C. By comparing the temperature change in the membrane with and without GNSs, it can be concluded that the irradiated GNSs caused a temperature increase by around 4 °C in the tBLMs when the electrode was not exposed to the horizontal laser beam.

The horizontal laser direction was applied in the experiment, in order to minimise the impact of the gold electrode on the heat generation in the irradiated samples. The correspondence between the temperature change and the conductance of the membranes measured when the GNPs were illuminated by a horizontal laser beam seen in Figure 11. It can be seen that the trend of temperature increase and decrease in Figure 11 is comparable to the change of conductance. The correlation between the temperature change and the ionic conductance of the membranes can be explained by the Arrhenius Law [30] and suggests that heat transfer induces the creation of transient membrane pores.

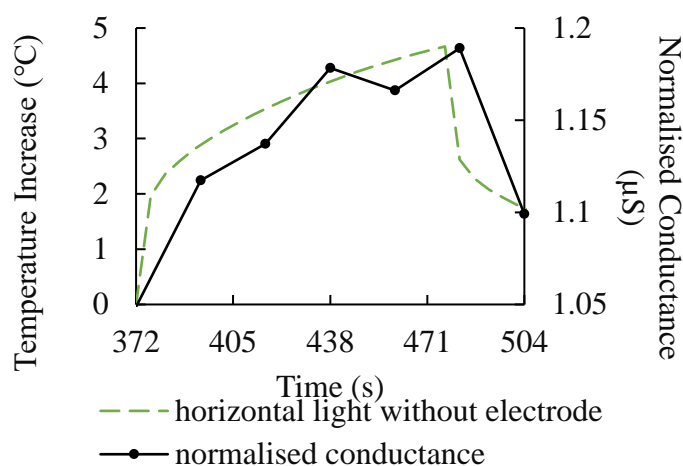


Figure 11 Temperature change of the membrane during and after the laser illumination.

6. CONCLUSIONS

Since the heating efficiencies of GNP aggregation structures depend on their sizes and the internal particle configuration, the optical properties of the GNP aggregate structures have been considered. Based on the structures of particle aggregates present in acidic solutions the weight averaged absorbance was calculated. A good agreement was established between the numerical predictions and published experimental results.

The temperature increases of GNP solutions at different pH levels was experimentally investigated using light irradiation. A clear positive correlation between the maximum temperature increase and the predicted absorbance of the GNP solution has been observed. It is evident that the present approach is capable of characterizing the impact of GNP aggregation behaviors on the optical absorption and heating efficiency of GNP solutions irradiated by NIR light. The results of the current investigation are helpful for medical practitioners to better understand the effect of particle aggregation on the performance in treatment procedures using GNP solutions, and how to control the particle aggregation by adjusting base fluid pH levels.

In addition, the heat transfer between GNPs and Tethered Bilayer Lipid Membranes (tBLMs) was numerically modelled to understand the effects of GNP hyperthermia on living cells membranes. The predicted temperature change was compared with the variation of membrane conductance of the tBLMs. The predicted results showed that the temperature in the tethered membrane increased by 4 °C when the GNSs adjacent to the membrane were irradiated by the laser beam. The correlation of temperature change with an increase in membrane conductance suggests that heat transfer induces the creation of transient membrane pores and/or induces existing intrinsic membrane pores to be widened. We demonstrated that the lipid bilayer membrane can be affected by conjugated GNP induced hyperthermia when irradiated with a laser.

REFERENCES

- [1] Svaasand, L.O.; Gomer, C.J.; Morinelli, E. On the physical rationale of laser induced hyperthermia. *Lasers in Med. Science* 1990, **5** (1990), 121–128, doi:10.1007/BF02031373.
- [2] Huang, X.; El-Sayed, M.A. Plasmonic photo-thermal therapy (PPTT). *Alexandria J. of Med.*, **47** (2011), 1–9.
- [3] Alves, A.; Mendo, S.; Ferreira, L.; Mendonça, M.; Ferreira, P.; Godinho, M.; Cruz, M.; Carvalho, M. Gelatine-assisted synthesis of magnetite nanoparticles for magnetic hyperthermia. *J. Nanopart. Res.*, **18** (2016), 1–13.

- [4] Taylor, R.; Coulombe, S.; Otanicar, T.; Phelan, P.; Gunawan, A.; Lv, W.; Rosengarten, G.; Prasher, R.; Tyagi, H. Small particles, big impacts: A review of the diverse applications of nanofluids. *J. Appl. Phys.*, **113** (2013), 1.
- [5] Thovhogi, N.; Sibuyi, N.; Meyer, M.; Onani, M.; Madiehe, A. Targeted delivery using peptide-functionalised gold nanoparticles to white adipose tissues of obese rats. *J. Nanopart. Res.* **17** (2015) 112–120.
- [6] Huang, X.; Neretina, S.; El-Sayed, M.A. Gold nanorods: From synthesis and properties to biological and biomedical applications. *Adv. Mater.*, **21** (2009), 4880-4910.
- [7] Huang, X.; El-Sayed, M.A. Gold nanoparticles: Optical properties and implementations in cancer diagnosis and photothermal therapy. *Journal of Advanced Research* **1** (2010), 13-28.
- [8] Gu, X., Timchenko, V., Heng Yeoh, G., Dombrovsky, L. and Taylor, R., The Effect of Gold Nanorods Clustering on Near-Infrared Radiation Absorption. *Applied Sciences*, **8**(2018), 1132
- [9] Pissuwan, D.; Valenzuela, S.M.; Miller, C.M.; Killingsworth, M.C.; Cortie, M.B. Destruction and Control of *Toxoplasma gondii* Tachyzoites Using Gold Nanosphere/Antibody Conjugates. *Small*, **5** (2009), 1030–1034
- [10] Hainfeld, J.F.; Lin, L.; Slatkin, D.N.; Dilmanian, F.A.; Vadas, T.M.; Smilowitz, H.M. Gold nanoparticle hyperthermia reduces radiotherapy dose. *Nanomedicine: Nanotechnology, Biology and Medicine*, **10** (2014), 1609–1617.
- [11] Dombrovsky, L. A., Timchenko, V., Jackson, M and Yeoh, G. A combined transient thermal model for laser hyperthermia of tumors with embedded gold nanoshells, *International Journal of Heat and Mass Transfer*, **54** (2011), 5459-5469.
- [12] Dombrovsky, L. A., Timchenko, V., and Jackson, M., "Indirect heating strategy for laser induced hyperthermia: An advanced thermal model," *Int. J. of Heat and Mass Transfer*, **55** (2012), 4688-4700.
- [13] Cornell, B. A. *et al.*, "Ion Channel Proteins that Spontaneously Insert into Lipid Bilayer Membranes: An Impedance Spectroscopy Study Employing Tethered Membranes," *Biophysical Journal*, **102** (2012) 682-683
- [14] Alghalayinia, A, Jianga L., Gub X.,, Yeoh, G., Cranfield, C., Timchenko, V., Cornell, B., Valenzuela, S., Real-time monitoring of heat transfer between gold nanoparticles and tethered bilayer lipid membranes, *BBA-Biomembranes* **1862** (2020) 183334
- [15] Dombrovsky, L. A., *Radiation heat transfer in disperse systems*. Begell House (1996), New York.
- [16] DeVoe, H. Optical properties of molecular aggregates. I. Classical model of electronic absorption and refraction. *J. Chem. Phys.*, **41** (1964), 393–400.
- [17] Draine, B.T.; Flatau, P.J. User guide for the discrete dipole approximation code DDSCAT 7.3. *arXiv preprint arXiv:1305.6497* (2013).
- [18] Jain, P.K.; Eustis, S.; El-Sayed, M.A. Plasmon coupling in nanorod assemblies: Optical absorption, discrete dipole approximation simulation, and exciton-coupling model. *J. Phys. Chem. B*, **110** (2006), 18243–18253.
- [19] Modest, M.F. *Radiative Heat Transfer*, Second edition, Acad. Press, (2003), New York.
- [20] Dombrovsky, L.A. and Baillis, D. *Thermal Radiation in Disperse Systems: An Engineering Approach*, Begell House, (2010), New York and Redding (CT).
- [21] Pennes, H.H. Analysis of Tissue and Arterial Blood Temperature in the Resting Human Forearm, *J. Appl. Physiol.*, **1** (1948), 93-122.
- [22] Khaled, A.-R.A. and Vafai, K., The Role of Porous Media in Modeling Flow and Heat Transfer in Biological Tissues, *Int. J. Heat Mass Transfer*, **46** (2003), No. 26, pp 4989-5003.
- [23] Peng, Z.; Walther, T.; Kleinermanns, K. Influence of intense pulsed laser irradiation on optical and morphological properties of gold nanoparticle aggregates produced by surface acid– base reactions. *Langmuir*, **21** (2005), 4249–4253.
- [24] Li, D.D.; Gu, X.; Timchenko, V.; Chan, Q.N.; Yuen, A.C.; Yeoh, G.H. Study of morphology and optical properties of gold nanoparticle aggregates under different pH conditions. *Langmuir*, **34** (2018), 10340–10352.
- [25] Randrianalisoa, J., Li, X., Serre, M., and Qin, Z., "Understanding the Collective Optical Properties of Complex Plasmonic Vesicles," *Advanced Optical Materials*, **5** (2017), 1700403
- [26] Dombrovsky, L.A.; Timchenko, V.; Pathak, C.; Piazena, H.; Müller, W.; Jackson, M. Radiative heating of superficial human tissues with the use of water-filtered infrared-A radiation: A computational modeling. *Int. J. Heat Mass Transfer*, **85** (2015), 311–320.
- [27] Zhang, M.; Kim, H.S.; Jin, T.; Moon, W.K. Near-infrared photothermal therapy using EGFR-targeted gold nanoparticles increases autophagic cell death in breast cancer. *J. Photochem. Photobiol. B: Biol.*, **170** (2017), 58–64.

- [28] Krishna, G., Schulte, J., Cornell, B. A., Pace, R. J., and Osman, P. D., "Tethered bilayer membranes containing ionic reservoirs: selectivity and conductance," *Langmuir*, **19** (2003), 2294-2305.
- [29] Cranfield, C., Carne, S., Martinac, B., and Cornell, B., "The assembly and use of tethered bilayer lipid membranes (tBLMs)," in *Methods in Membrane Lipids*: Springer, (2015), 45-53.
- [30] Birngruber, R., "Thermal modeling in biological tissues," in *Lasers in Biology and Medicine*: Springer, (1980), 77-97.
- [31] Pope, R. M. and Fry, E. S., "Absorption spectrum (380–700 nm) of pure water. II. Integrating cavity measurements," *Applied optics*, **36** (1997), 8710-8723.
- [32] Jain, P. K., Lee, K. S., El-Sayed, I. H., and El-Sayed, M. A., "Calculated absorption and scattering properties of gold nanoparticles of different size, shape, and composition: applications in biological imaging and biomedicine," *Journal of Physical Chemistry B*, **110** (2006), 7238-7248.
- [33] Lee, V. and Tarassenko, L., "Absorption and multiple scattering by suspensions of aligned red blood cells," *JOSA A*, **8** (1991), 1135-1141.
- [34] Axelevitch, A., Apter, B., and Golan, G., "Simulation and experimental investigation of optical transparency in gold island films," *Optics express*, **21** (2013), 4126-4138.